Simulation study of the electrical yield of various PV module topologies in partially shaded urban scenarios

Calcabrini, Andres; Weegink, Raoul ; Manganiello, Patrizio; Zeman, Miro ; Isabella, Olindo

DOI
10.1016/j.solener.2021.07.061

Publication date
2021

Document Version
Final published version

Published in
Solar Energy

Citation (APA)
Calcabrini, A., Weegink, R., Manganiello, P., Zeman, M., & Isabella, O. (2021). Simulation study of the electrical yield of various PV module topologies in partially shaded urban scenarios. *Solar Energy*, *225*, 726-733. https://doi.org/10.1016/j.solener.2021.07.061

Solar Energy 225 (2021) 726–733

Contents lists available at ScienceDirect

Solar Energy

journal homepage: www.elsevier.com/locate/solener

Simulation study of the electrical yield of various PV module topologies in partially shaded urban scenarios

Andres Calcabrini *, Raoul Weegink, Patrizio Manganiello, Miro Zeman, Olindo Isabella

Department of Electrical Sustainable Energy, Delft University of Technology, 2628CD, Delft, The Netherlands

ARTICLE INFO

Keywords:
PV module topology
Urban PV systems
Bypass diodes
Partial shading
Shading tolerance

ABSTRACT

Urban environments present a great potential to generate electricity with photovoltaic technology. However, this electricity cannot be fully harvested using conventional solar modules that have been designed for open landscapes. In urban environments, photovoltaic modules can often be subject to partial shading caused by trees and building structures. Therefore, new photovoltaic module concepts and designs must be explored to increase the shading tolerance of PV modules. This study proposes a simple yet effective approach to compare the potential of different module topologies for maximising the electrical yield of partially shaded photovoltaic systems. Using this approach, the annual electrical performance of various PV module topologies in different urban environments and climates is simulated and compared to determine the potential benefit of using photovoltaic modules with new topologies. Results suggest that the shading tolerance of conventional solar modules can be significantly improved by adding only a few bypass diodes or parallel interconnections. It is shown that the yield of a partially shaded PV system endowed with conventional solar modules could be increased as much as 25% when shading is caused by nearby obstructions.

1. Introduction

The deployment of photovoltaic (PV) systems in urban environments has the potential to supply a significant share of the urban energy demand and to make a positive impact on different aspects of urban sustainability (Kammen and Sunter, 2016). Nevertheless, while utility-scale PV power generation continues breaking price records (IRENA, 2018), the average levelised cost of electricity (LCOE) of residential solar PV is still three times higher (Kost et al., 2018; Jäger-Waldau, 2019). The large disparity in LCOE is mainly due to (i) the scale difference between utility and residential PV plants, and (ii) the characteristics of the solar potential in urban landscapes, which is uneven and ever-changing due to surrounding buildings, trees and other structures (Jahn and Nasse, 2004). In this context, the development of shade resilient PV modules can contribute to reduce the cost and increase the energy potential of urban PV systems.

Nowadays, the dominant photovoltaic module technology in the market is crystalline silicon (c-Si). Many different c-Si modules, which differ in cell technology and structure, number of cells, encapsulation, frame design, etc., are readily available. Despite these differences, the electrical interconnections between the cells in most commercial PV modules is a common denominator: most PV modules have all their solar cells connected in series which allows to keep the output currents low and thereby minimise conduction losses.

Typically, PV modules also include bypass diodes to prevent hot-spots (Silvestre et al., 2009) and limit the effect of shading on the module output power. Conventional c-Si modules consist of 60 (or 72) series-connected solar cells arranged in 3 sub-strings, where each sub-string is a group of 20 (or 24) series-connected cells under the same bypass diode. The way in which diodes are connected to the solar cells is most effective in the case of row-to-row shading in large PV power plants, when proper installation ensures that the shadow is parallel to the longer edge of the module. However, in the urban environment, chimneys, dormers, buildings, trees, fouling, etc., usually cast complex time- and shape-varying shadows on the modules, which result in a poor electrical performance of the PV system.

During clear sky days, the irradiance on the unshaded solar cells in a module can be one order of magnitude higher than the irradiance on the shaded solar cells. When there is irradiance mismatch between cells, conventional modules perform poorly because the breakdown voltage of typical front–back contacted c-Si solar cells is between −10 V and −20 V (Bauer et al., 2013). As a consequence, if a cell in a sub-string is shaded, the cell is driven into reverse bias operation and limits the current flow. Depending on the operating current of the PV module,

* Corresponding author.
E-mail addresses: a.calcabrini-1@tudelft.nl (A. Calcabrini), r.weegink@student.tudelft.nl (R. Weegink), p.manganiello@tudelft.nl (P. Manganiello), m.zeman@tudelft.nl (M. Zeman), o.isabella@tudelft.nl (O. Isabella).

https://doi.org/10.1016/j.solener.2021.07.061
Received 11 November 2020; Received in revised form 2 July 2021; Accepted 26 July 2021
Available online 5 August 2021

one shaded cell can cause the inversion of the voltage across the entire sub-string. In this situation, the bypass diode conducts the additional electrical current generated by the unshaded sub-strings in the module and allows the module to generate more electrical power. Nonetheless, the use of bypass diodes also has its downsides: the output power of a conventional PV module can drop by more than 30 % even when less than 1 % of the area of a PV module is shaded (Sinapis et al., 2016).

The first alternative to improve the electrical yield of partially shaded PV systems consists in using module level power electronics (MLPE). MLPE devices, including micro-inverters (Deline et al., 2012) and DC power optimisers (MacAlpine et al., 2012), allow to independently maximise the output power of every PV module in the system. This solution can significantly improve the performance of a PV system compared to the case where modules are connected in series to a single string-level maximum power point tracking device.

To increase the energy yield of partially shaded PV systems even further, the design of the PV module must be modified. For example, the shading resilience of an individual solar module can be improved by adding more bypass diodes. In Pannebakker et al. (2017) the authors explain how the shading tolerance of a series-connected PV module can be raised by increasing the number of bypass diodes in a module and replacing bypass diodes with active bypass elements (e.g., smart bypass diodes). Furthermore, a recent study, shows that PV modules manufactured with one bypass diode per cell can deliver 80 % more power than a conventional PV module when a row of cells is shaded (Hanifi et al., 2019). However, it is yet unclear how much additional electrical energy solar modules with multiple bypass diodes can generate in realistic scenarios compared to conventional modules throughout a year. This evaluation is complex since it requires the monitoring of different PV module topologies in different shading scenarios for long periods of time.

A different approach for increasing the shading tolerance of PV modules consists in connecting solar cells in parallel. While the relation between the maximum power point current and the illumination level is almost linear, the relation between the maximum power point voltage and the incident irradiance is logarithmic (Chegaar et al., 2013). As a result, parallel connections of solar cells are more shade tolerant than series connections. The most common configurations with parallel connections are series–parallel (SP) and total-cross-tied (TCT) modules. An example of a SP module is the Tessera module, which consists of 15 parallel-connected building blocks, each block made of 64 series-connected sub-cells grouped in 4 units, each unit protected by a bypass diode (Carr et al., 2015). Series–parallel connections are also present in half-cut cell modules which perform better than conventional PV modules under partial shading conditions (Lu et al., 2013; Hanifi et al., 2015). On the other hand, total-cross-tied configurations offer similar advantages to SP topologies but since they generally deliver power at higher current levels, this electrical configuration is commonly applied to system-level interconnections (Mohammadnejad et al., 2016).

Previous research on the evaluation of shading tolerance of PV modules (Pannebakker et al., 2017; Hasyim et al., 1986; Ziar et al., 2017; Mittag et al., 2019; Lefevre et al., 2017; Mishra et al., 2019) focuses either on the performance of a single (or few) innovative PV module topologies and/or on the evaluation of the power increase in specific shading cases (e.g. row shading, corner shading) at specific time instants and for short time periods (few days at most). The main reason for such a limited analysis is the excessive computational time needed for a thorough and fair comparison.

In this paper, we present a methodology for comparing many shade tolerant PV module topologies in terms of annual DC yield gain (or loss) in realistic shading scenarios. Yearlong comparison represents a huge advantage, since our approach considers the probability of occurrence of different shading patterns during an entire year. This article is organized as follows. In Section 2, the study cases are described. In Section 3, the general simulation framework is introduced. In Section 4, the proposed methodology for evaluation of different module topologies is presented and validated through comparison with the highly accurate but computational demanding simulation approach from Section 3, to demonstrate its ability to reduce the computational time while allowing for proper performance comparison. In Section 5, the developed methodology is used to compare the annual performance of 49 different PV module topologies, installed on two different rooftops under 3 different climate conditions. It is shown that the proposed methodology overcomes the limitation of up-to-date literature approaches and is a valuable tool that can be used by PV module designers first and architects later to come up with novel module topologies optimised for operation in partially shaded (urban) scenarios. Conclusions end the paper.

Table 1
Solar resources in each of the 3 locations analysed. The irradiation values in the table correspond to the annual global horizontal irradiation. The cloud cover values correspond to the annual average cloudiness during daytime.

City	Rotterdam (NL)	San Francisco (US)	Bogotá (CO)
Latitude (°)	51.9	37.2	4.6
Irradiation (MWh m^{-2})	1.02	1.71	1.57
Cloud cover (okta)	5.6	3.3	5.9

2. Study cases

2.1. Shading scenarios

Two rooftops were chosen to carry out this simulation study. These "shading scenarios", reconstructed using photogrammetry data from actual buildings, are shown in Fig. 1. On the red rooftops in Figs. 1a and 1d, a 156-mm spaced squared grid was generated to compute the irradiance on each cell. In turn, the squared cells on the rooftop were grouped to define modules with 72 cells (organised in a 6-by-12 layout). Furthermore, on each rooftop two scenarios are considered in which modules are either mounted in landscape or portrait orientation. In total, considering the four presented cases, 137 PV module positions are analysed.

The shadows on each rooftop have different characteristics. Rooftop 1 (RT1) is facing Southwest and shading is mainly caused by two chimneys. Due to the short distance from the rooftop to the chimneys, shadows are relatively small and move slowly on the PV array. The edges of the shadows are sharp and during clear sky days there is a large irradiance difference between the shaded and unshaded sectors of the roof. On the other hand, Rooftop 2 (RT2) is facing East and shadows are mostly caused by the tall building in front of the rooftop, which is about 30 m away. In this case, shadows, which occur during the morning, move faster on the rooftop and the edges of the shadows are more diffuse. Also, the irradiance difference between shaded and unshaded parts of the rooftop is less pronounced than in the case of RT1.

Furthermore, it is considered that these rooftops can be found in three different cities, for which 10-minute resolution climate data was downloaded from Meteonorm (Remund et al., 2020). All the locations considered are in the northern hemisphere but the available solar resources in each place differ significantly as shown in Table 1.

2.2. Module topologies

As mentioned in Section 2.1, PV modules made of 72 cells organised in a 6-by-12 layout are considered in this study. Contiguous cells can be grouped together to form different module layouts. In this analysis, the 24 module layouts shown in Fig. 2 have been evaluated. Furthermore, two different types of electrical interconnections were evaluated for each PV module layout: (1) modules with bypass diodes (BPD), in which all cells in the PV module are connected in series and each group has its own bypass diode; and (2) series–parallel modules (SP),

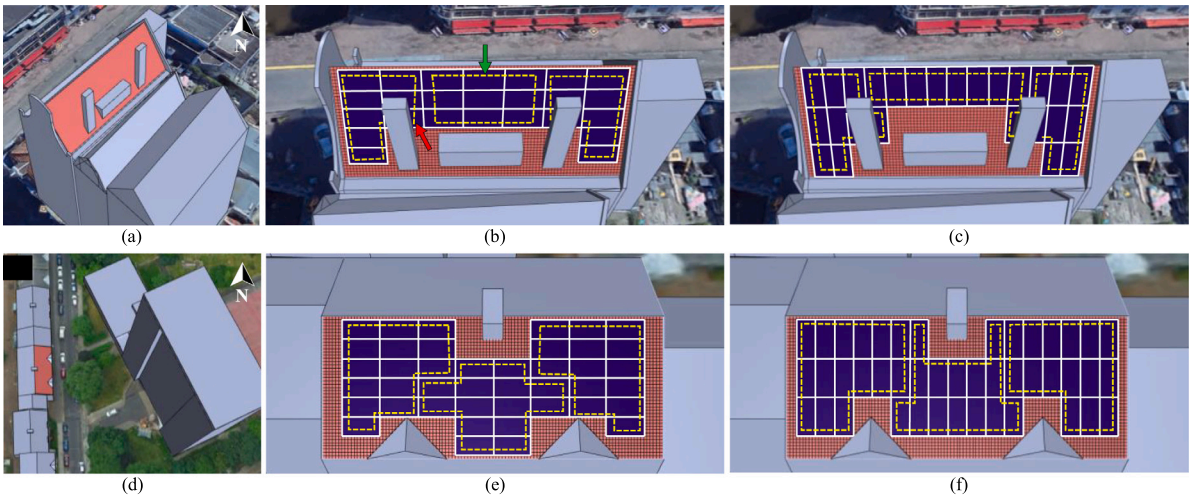

Fig. 1. Simulated PV installations. (a) Rooftop 1 (RT1): The roof is tiled 57° and facing almost Southwest (214° clockwise from North). Shading is mostly caused by the chimneys on the roof and by the adjacent buildings. (b) PV array with 25 modules mounted in landscape on RT1. The green and the red arrows indicate the least and most partially shaded PV modules in the array, respectively, considering the climate of Rotterdam. (c) PV array with 26 modules mounted in portrait on RT1. (d) Rooftop 2 (RT2): The roof is tilted 30° and facing almost to the East (100° clockwise from North). Shading is mostly caused by the tall building in front the rooftop. (e) PV array with 42 modules mounted in landscape on RT2. (f) PV array with 44 modules mounted in portrait on RT2.

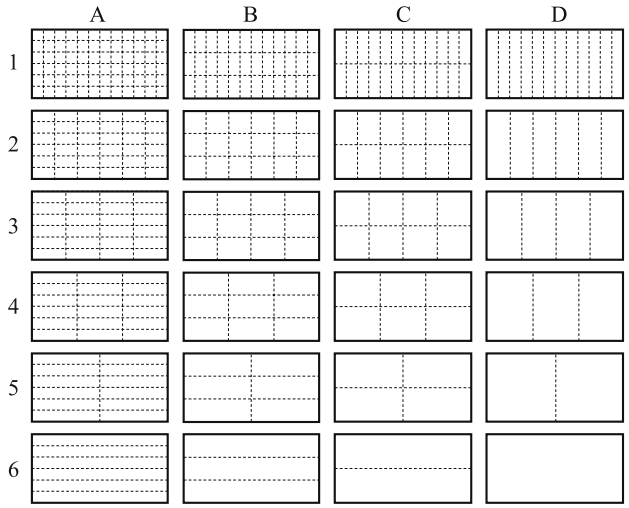

Fig. 2. Analysed module layouts. Each layout is identified by a letter (column) and a number (row). In total 24 different layouts have been studied, each consisting of a matrix of 6 by 12 solar cells. Dashed lines separate different groups of cells in the module.

in which cells within a group are connected in series and all groups are connected in parallel (without bypass diodes). Therefore, 48 different PV module topologies have been simulated[1].

According to the notation defined in Fig. 2, B6-BPD is the topology of a conventional 72-cell c-Si PV module with 3 bypass diodes; A1-BPD is equivalent to the Smart Hot-Spot Free module by AE Solar (Solar, 2019); and B3-SP is similar to the Tessera module (Eerenstein et al., 2015). It is worth mentioning that (i) the Tessera module is made of 60 cells; and (ii) that each cell is cut into 16 sub-cells and then connected in series to reduce cell-to-module losses forming 15 series–parallel groups of cells. Therefore, the shade response of the Tessera module and layout B3-SP are not exactly the same.

[1] Total-cross-tied PV modules were also evaluated. For the sake of simplicity and since results were comparable to the ones obtained with SP modules, we have decided not include TCT results in this work.

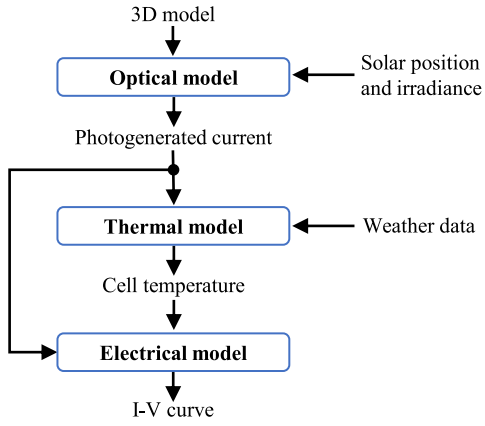

Fig. 3. Block diagram of the modelling framework used to simulate the I–V curve of solar cells.

In addition to the 48 module topologies already mentioned, the performance of 144-half-cut cells PV modules (HC) was also evaluated. The topology of a half-cut cell PV module can be described as a series–parallel–series module with bypass diodes and should not be confused with B5-BPD in which all groups of cells are connected in series, nor with B5-SP in which all groups of cells are connected in parallel with each other.

3. Simulation framework

The DC energy yield of a PV array was simulated with a framework that combines 3 models as shown in Fig. 3: (1) an optical model to determine the photo-generated current of each solar cell in the module; (2) a thermal model to calculate the temperature of each solar cell; and (3) an electrical model to generate the I–V curve of the module and obtain the power delivered at the maximum power point. High accuracy of the simulation can be ensured by using experimentally validated models.

The optical model used in this work is the forward ray-tracing model proposed in Santbergen et al. (2017). To determine the irradiance incident on the cells, first a 3D model of the PV modules and its surroundings is created. For simplicity, it is assumed that all the

surfaces surrounding the PV modules are ideal diffuse reflectors with an albedo of 0.15. Then, sensitivity maps for each cell on the rooftop are generated using a ray-tracing engine. Lastly, the sensitivity maps, which quantify the fraction of the radiance emitted by each sky sector and received by the solar cell (Santbergen et al., 2017), are multiplied with sky maps generated with Perez model (Perez et al., 1993) to calculate the irradiance and the photo-generated current of each solar cell at every time instant.

Once the irradiance is determined, the Faiman model is used to calculate the cell temperature (Faiman, 2008). Only for the temperature calculation, it is assumed that each cell is operated at its maximum power point, which allows to decouple the thermal and electrical models. It is also assumed that heat transfer between cells within the module is negligible. It is also considered that module lamination is glass/foil and that the back side of the module is thermally insulated. The thermal constants for Faiman model used in this work ($U_0 = 14.4\,\mathrm{W\,m^{-2}\,K^{-1}}$ and $U_1 = 0.034\,\mathrm{W\,m^{-3}\,s^{-1}\,K^{-1}}$) are derived from the empirical coefficients reported in King et al. (2004b).

Knowing the cell temperature and the photo-generated current, the I–V characteristics of solar cells are simulated using the 2-diode electrical equivalent model (Wolf et al., 1977; Charles et al., 1985; Chan and Phang, 1987). It is considered that both the series and parallel resistances are temperature independent, and the diode saturation current varies with cell temperature T as described in Ishaque et al. (2011). Finally, the I–V curves of the cells are added together to calculate the I–V curve of the entire PV module. In this last step, the losses in the interconnecting tabs are modelled as an additional resistance connected in series to each solar cell, and the losses in the bypass diodes (Texas Instruments, 2012) are calculated considering the I–V characteristics at 25 °C.

4. I-V curve approximation

To perform a fair assessment of the 49 different module topologies for the case studies presented in Section 2, the I–V curves at 137 PV module positions are simulated using 3 climate data sets. Considering that it takes about 6 minutes to simulate the annual I–V curves of a single module with a 10-minute time step (on a PC with a 4-core Intel Xeon E5-1620 CPU with 16 GB of RAM), the simulation of all possible combinations using the highly accurate simulation framework presented above would take about three consecutive months. In order to reduce the computational time and perform a fair and reliable relative comparison between PV module topologies, the simulation framework presented above has been adapted. Specifically, the two-diode electrical model has been replaced with a squared approximation.

4.1. The squared approximation

Essentially, the proposed approximation considers that the fill factor of the cell is 100 %, and hence the maximum power point of the solar cell is determined by the short-circuit current and the open-circuit voltage. The short-circuit current of the solar cell at any given irradiance G and cell temperature T, depends on the temperature difference from Standard Test Conditions (STC) conditions ΔT and the temperature coefficient of the short-circuit current α according to Chenni et al. (2007):

$$I_{sc}(G,T) = I_{sc0}\,\frac{G}{G_0}\,(1+\alpha\,\Delta T)\,. \tag{1}$$

On the other hand, the open-circuit voltage at any given irradiance and temperature is defined similarly as in King et al. (2004a):

$$V_{oc}(G,T) = V_{oc0} + \delta\,\ln\left(\frac{G}{G_0}\right) + \beta\,\Delta T, \tag{2}$$

where β is the temperature coefficient of the open-circuit voltage. Two minor simplifications on the original model are made: the parameter δ is the product between the thermal voltage at STC and the ideality factor of the solar cell; and the ratio between G and G_0 neglects the slight variations in the number of photo-generated carriers at different temperatures.

Table 2
Solar cell parameters.

η_0 (%)	FF_0 (%)	I_{sc0} (A)	V_{oc0} (V)	α (1/K)	β (mV/K)	δ (mV)
19.48	79.5	9.345	0.638	0.0005	−1.9	27.2

It is considered that when N_s solar cells are connected in series, the short-circuit current of the string is equal to the short-circuit current of the least illuminated cell and the open circuit voltage can be calculated as:

$$V_{oc\text{-}s} = N_s\,V_{oc0} + \delta\,\ln\left(\prod_{i=1}^{N_s}\frac{G_i}{G_0}\right) + \beta\sum_{i=1}^{N_s}\Delta T_i. \tag{3}$$

Likewise, when N_p cells are connected in parallel, the voltage is limited by the least illuminated solar cell and the short-circuit current is given by:

$$I_{sc\text{-}p} = \frac{I_{sc0}}{G_0}\left(\sum_{i=1}^{N_p} G_i + \alpha\sum_{i=1}^{N_p} G_i\,\Delta T_i\right). \tag{4}$$

Eqs. (3) and (4) can be combined to calculate the squared approximation of the I–V curve of any PV module topology. Despite the squared approximation resulting in an overestimation of the annual yield, it allows to reduce the simulation time by at least two orders of magnitude, depending on the computer hardware. In the following section, the suitability of the squared approximation to make a relative comparison between different topologies is discussed.

4.2. Validity of the squared approximation

It is clear that the deviations of the squared approximation from the actual I–V curve of a solar module are smaller for modules with higher fill-factors. Since the fill-factor of modern commercially available c-Si PV modules is close to 80 %, the deviations between the squared approximation and the 2-diode model for different module topologies have been analysed.

The simulation results presented in this paper were obtained using the c-Si solar cells presented in Hanifi et al. (2016). The external parameters and the temperature coefficients of the simulated solar cells used in the squared approximation are summarised in Table 2.

A comparison between the DC yield obtained using the 2-diode equivalent model and the squared approximation for different module layouts is presented in Figs. 4a (for topologies with bypass diodes) and 4b (for series–parallel topologies) for the most shaded module in the array in Fig. 2b using climate data for Rotterdam. This module is subject to partial shading about 50 % of the time in the year. Blue circles in Fig. 4 refer to simulations performed with the 2-diode electrical model, whereas orange squares refer to simulations performed using the squared approximation. In this case, results indicate that most module topologies would perform significantly better than the conventional topology. For example, the plot in Fig. 4a shows that, according to the 2-diode model, the annual DC yield of the most shaded module can be boosted almost by 45 % when using modules with one bypass diode per cell (A1-BPD) compared to a conventional module (B6-BPD). It can also be noticed that, since shadows on the analysed position on the roof mostly move from left to right, module D4-BPD (which also has 3 bypass diodes) and the half-cut cell module (HC) can deliver about 25 % more energy than module B6-BPD. This examplifies the the importance of the mounting orientation. The relative gain calculated with the squared approximation shows good correlations with the results from the 2-diode model. Deviations are larger for the best performing module

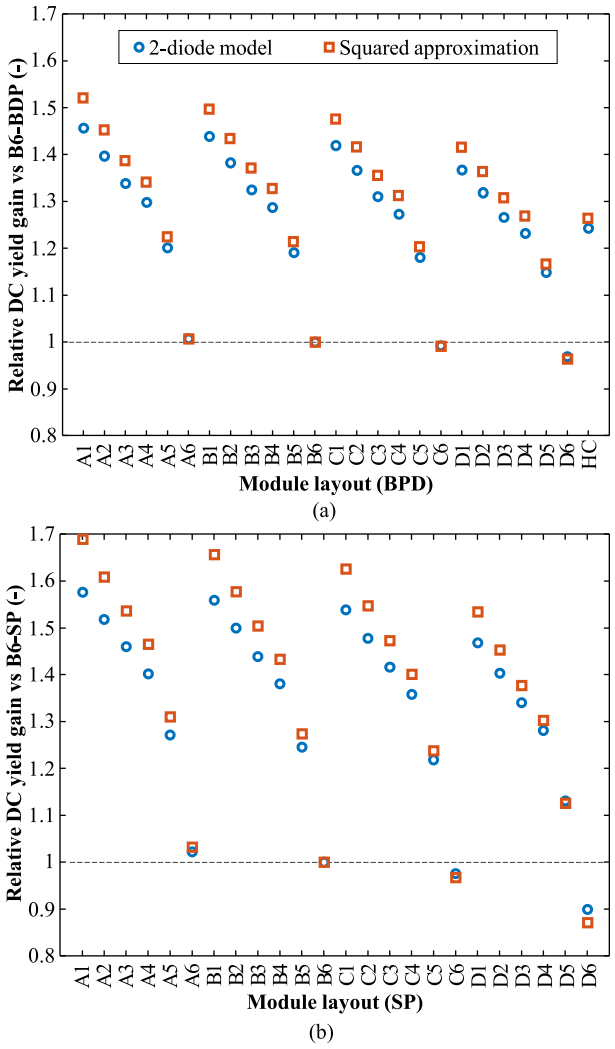

Fig. 4. Relative DC yield gain relative to module layout B6 for the most shaded PV module on RT1 in Rotterdam. (a) Comparison between BPD topologies and layout B6-BPD. The plot also shows a comparison between the half-cell module (HC) and topology B6-BPD. (b) Comparison between SP topologies and layout B6-SP.

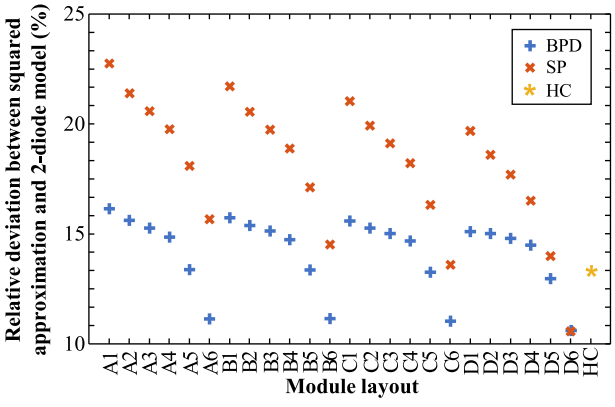

Fig. 5. Relative deviation between the squared approximation and the 2-diode equivalent model in the worst-case scenario (the most shaded PV module on RT1 in Rotterdam).

topologies, yet the maximum deviation (module A1-SP) is only 11.3 % in Fig. 4b.

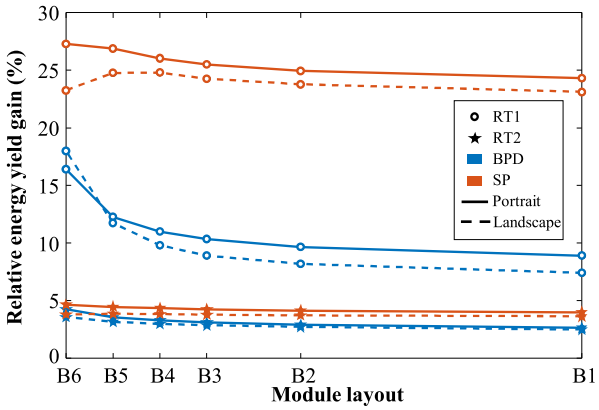

Fig. 6. Relative energy yield gain in Rotterdam when replacing a central inverter by module level power electronics in the installations in Fig. 1. Layouts on the horizontal axis are spaced according to the corresponding number of bypass diodes or parallel groups of cells.

Fig. 5 gives a better picture of the deviations between the squared approximation and the 2-diode model. Since the squared approximation is only intended to make relative comparisons between topologies, ideally, the deviation for all the BPD and SP layouts should be the same but not necessarily zero. In Fig. 5, layout D6 left aside[2], the dispersion of deviations between BPD topologies is roughly 5 % (from A1-BPD to C6-BPD) and between the SP topologies is about 9 % (from A1-SP to C6-SP). It should be noted that the deviations in the SP case are larger than in the BPD case because the difference between the squared approximation and the actual I–V curve of a partially shaded module increases with the number of parallel-connected solar cells.

It is important to mention, that plots in Figs. 4 and 5 were generated considering the worst-case scenario, i.e. the most shaded PV module on the array. If instead the least shaded PV module in the array in Fig. 1b is considered, which is shaded only 6 % of the year in Rotterdam, deviations range between 21.2 % and 21.7 % for BPD layouts and between 22.3 % and 24.9 % for the SP layouts. This means that the maximum difference between the squared approximation and the 2-diode model is only 0.5 % and 2.6 % for the BPD and SP layouts, respectively. Consequently, if the yield increase of entire PV systems in Fig. 1 is evaluated, the deviations introduced by the squared approximation will be between those of the most and least shaded modules.

5. Results and discussion

The squared approximation has been applied to compare different PV systems and module topologies based on the case studies presented in Section 2.

5.1. Central inverters vs MLPE

The energy yield of PV systems with central inverters was compared to PV systems with MLPE (i.e., micro-inverters or power optimisers) to quantify the benefits of performing MPPT at module level. For the PV systems with a central inverter, a typical inverter with 3 independent string inputs has been considered. The yellow dashed lines in Fig. 1 indicate which modules are connected in series forming the 3 strings in each of the analysed PV installations. Furthermore, it was considered that each PV module has at least one bypass diode and that central

[2] Both modules D6-BPD and D6-SP have all their solar cells connected in series (with no bypass diodes) and in practice partial shading would cause hot-spots and permanent damage of the PV module, hence this is not a configuration of interest.

inverter can independently maximise the power of each string. On the other hand, the energy yield of the PV systems with MLPE was calculated considering that the power output of each PV module is independently maximised by a dedicated converter.

The energy yield increase obtained in Rotterdam when replacing the central inverter by MLPE is shown in Fig. 6 for the layout family B (refer to Fig. 2). Results indicate a significant energy yield boost when using MLPE, especially for the installations on the most shaded rooftop (RT1). It can also be noticed that, for the same installation, the gain is always higher for SP topologies compared to BPD topologies because a partially shaded string of modules with parallel interconnections presents higher current mismatch losses than a string of modules with bypass diodes. Moreover, the clear decreasing trends in the BPD curves show that more shade tolerant PV modules (i.e., modules with more bypass diodes) allow to reduce the energy yield gap between systems with central inverters and systems with MLPE. In essence, increasing the number of bypass diodes per module is an effective approach to increase the shading tolerance of a PV system with a central inverter. On the other hand, the absence of a clear decreasing trend in the SP curves, suggests that MLPE is crucial to benefit from the improved shading tolerance offered series–parallel module topologies.

5.2. PV systems with MLPE

When PV modules are connected in series forming a string, the shading tolerance of the PV system is strongly constrained by the current mismatch between modules, regardless of the PV module topology. Instead, in PV systems with MLPE the shading tolerance of the PV system is mainly limited by the shading tolerance of the PV module topology. Thus, PV systems with MLPE were further analysed to make a fairer evaluation of the potential of different module topologies.

Fig. 7 presents a comparison of the annual DC yield gain obtained with different BPD module layouts in landscape orientation in different shading scenarios and locations. It can be noticed from the results in Fig. 7 that the conventional PV module (B6-BPD) is one of the poorest performing module topologies when a system is affected by partial shading. In particular, when shading objects are close to the PV modules as in RT1, increasing the number of bypass diodes can significantly increase the yield of a PV system, even at locations close to the Equator like Bogotá. In contrast, when shading is caused by large distant objects as in RT2, shadows are generally larger than the dimensions of a PV module, hence solar modules are rarely partially shaded. In such cases, MLPE provide sufficient shade resilience to the PV systems and using different module topologies can only marginally increase the annual DC yield.

Furthermore, all the plots in Fig. 7 show a clear tendency: the electrical performance of the system rapidly increases by adding additional bypass diodes but the trend flattens out around 12 diodes. For example, in RT1 in Rotterdam, 3 out of 4 topologies with 12 bypass diodes can boost the annual yield by 10 % compared to the conventional PV module, whereas a system with modules with 72 diodes (one per cell) can only produce 4 % additional energy. The reason why the trends start to flatten out around 12 BPDs is because all layouts with more than 12 groups of cells have at least two horizontal and two vertical divisions (see Fig. 2) which already provides them with high shading tolerance regardless the shape or direction of the shadows. In other words, for the given layouts and scenarios, increasing the granularity to more than 12 groups only slightly improve the performance.

It is worth mentioning, that the results in Fig. 7 were obtained considering ideal bypass diodes (i.e., zero forward voltage drop). This approximation is highly accurate for modules with active bypass diodes (Texas Instruments, 2012), however, adding too many bypass diodes can become disadvantageous when the forward voltage of the diodes is comparable to the voltage of the solar cell at the maximum power point. Losses in bypass diodes can be easily included in the proposed approximation by modifying Eq. (3).

Table 3
Relative DC yield gain of PV systems with half-cut cell modules compared to PV systems with conventional modules (B6-BPD).

	RT1 portrait (%)	RT1 landscape (%)	RT2 portrait (%)	RT2 landscape (%)
Rotterdam	7.4	10.2	0.83	0.71
San Francisco	6.8	10.0	0.87	0.90
Bogotá	6.3	6.1	0.55	0.58

Similar conclusions as for the case of landscape mounting can be drawn from the simulation results of systems with modules mounted in portrait. The main difference is that, in opposition to the landscape mounting case, for portrait mounting, A and D are the best and worst performing layout families, respectively. The reason is that shadows on the rooftops progress from left to right and in certain layouts bypass diodes are activated progressively, minimising the number of solar cells that are bypassed when the module is partially shaded. From another standpoint, layouts B and C are the best options when the shading direction is unknown.

A comparison considering SP topologies is presented in Fig. 8. Whereas the general trends are similar to those in Fig. 7, series–parallel modules in scenario RT1 can boost the gain about 10% more than modules with multiple bypass diodes. The trends in Fig. 8 also flatten out for modules with more than 12 groups connected in parallel for the same reason as in Fig. 7. In this case, more parallel-connected groups imply modules with lower output voltage and higher output current. While this could be problematic for the design of the power converter, in practice, series–parallel modules can be designed following the approach of the Tessera module (Carr et al., 2015), where each cell is cut into smaller sub-cells to reduce the string current and increase its voltage.

Finally, we also simulated the yield of systems with half-cut cell modules. The DC yield gains compared to the conventional module are summarised in Table 3. Results indicate that, in terms of shading tolerance, half-cut cells already represent a significant improvement with respect to conventional modules, yet there is room for improvement.

Certainly, improving the shading tolerability has an impact on the cost of PV modules. On the one hand, more bypass elements per module, especially active bypass elements with low voltage drops, imply higher material costs and introduce more peaks in the P–V curve, which might require the adaption of maximum power point tracking techniques in power converters. On the other hand, the design of series–parallel modules might require cutting the solar cells in smaller pieces and design of dedicated power converters able to operate in the voltage and current ranges of the module. The procedure proposed in this article allows to find the (Pareto) optimal module granularity, meaning a point in which increasing the number of groups (therefore the granularity) could lead to only a slight improvement of the performance while significantly increasing the complexity, and likely the cost, of the PV module. The trends presented in Figs. 7 and 8 can allow PV module manufacturers to make more thorough cost–benefit analysis of different module topologies. Moreover, the proposed methodology can be used to simulate PV module topologies that differ from the ones presented in this paper. Therefore, the same analysis can be replicated for any PV module topology of interest. Finally, a quick comparison between different module topologies can help architects and PV system designers to choose among different available PV modules in the market, and PV module manufacturers to create installation-specific PV modules.

6. Conclusions

Partial shading is ubiquitous in urban environments. Therefore, to increase the yield of urban PV systems and maximise the useable surface area for PV in the urban fabric, shade tolerant PV modules are required.

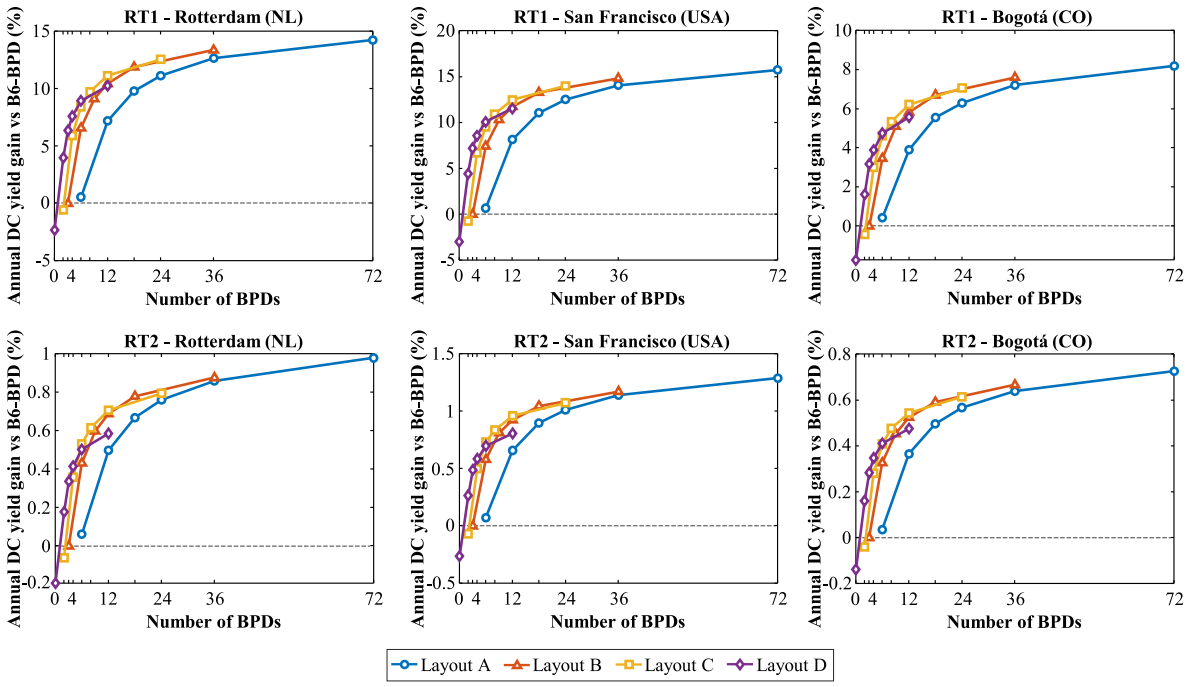

Fig. 7. Annual DC yield comparison for various BPD topologies. Results correspond to the case when modules are mounted in landscape orientation. The vertical axis in the plot indicates the energy yield increase with respect to the systems with B6-BPD modules.

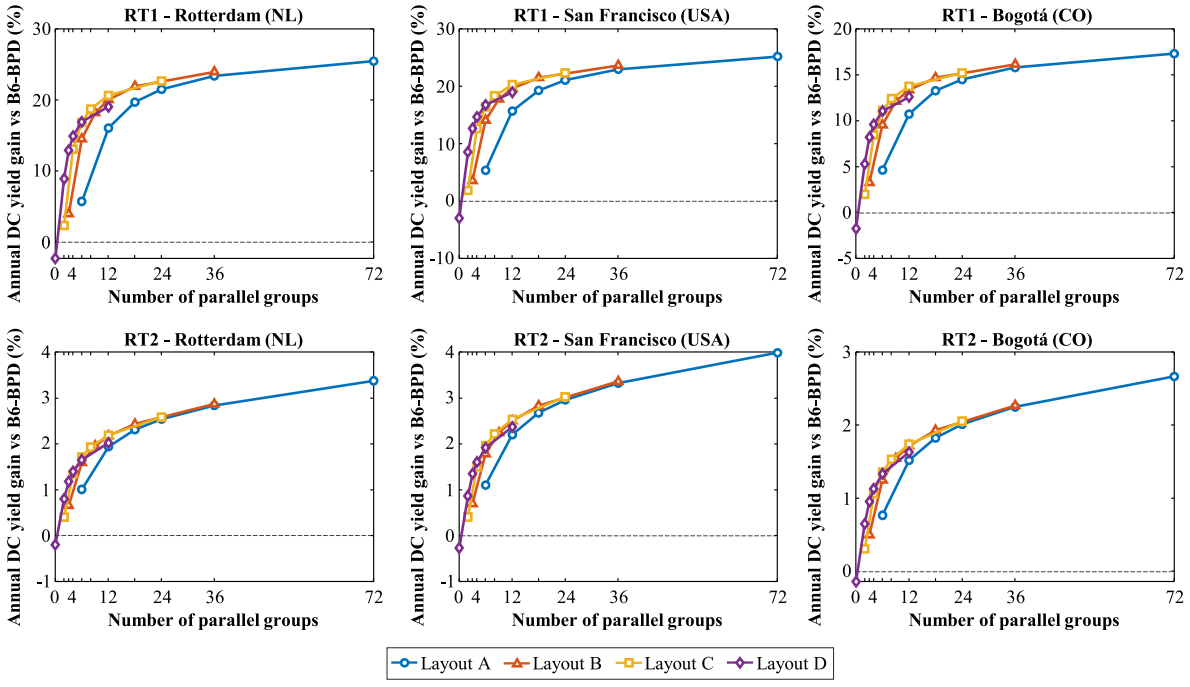

Fig. 8. Annual DC yield comparison for various SP topologies. Results correspond to the case when modules are mounted in landscape orientation. The vertical axis in the plot indicates the energy yield increase with respect to the systems with B6-BPD modules.

In this article, we have presented a simple and yet accurate approach to quickly compare the annual DC yield of PV systems with different PV module topologies. This approach allows to reduce by two orders of magnitude the simulation time of the two-diode electrical equivalent model. We evaluated 49 different module topologies, including some that are already commercially available, in different shading scenarios and climates. Our results suggest that when partial shading is caused by objects far from the PV modules, module level power electronics may be sufficient to provide shading tolerance to a PV system. However, when shading is caused by nearby objects, the module topology plays a determinant role in the electrical performance of the PV system.

From the analysis of different case studies, it is concluded that PV modules with one bypass element per cell could deliver between 8 % and 15 % more energy than a conventional module depending on the location given that the voltage drop on the bypass element is sufficiently low. Series–parallel topologies can improve the performance even more, increasing the yield up to 25 %. We also determined the gain

that can be expected from half-cut cell modules, which are becoming increasingly popular and could allow a partially shaded PV system to generate between 6 % and 10 % more energy in a year than with conventional PV modules. Finally, we found clear trends between the annual DC yield gain and the number of bypass elements and groups of parallel strings in a PV module topology. These clear trends can be very valuable for PV module manufacturing companies when performing cost–benefit analysis of new shade resilient PV module topologies.

Declaration of competing interest

The authors declare that they have no known competing financial interests or personal relationships that could have appeared to influence the work reported in this paper.

References

Bauer, J., Lausch, D., Blumtritt, H., Zakharov, N., Breitenstein, O., 2013. Avalanche breakdown in multicrystalline solar cells due to preferred phosphorous diffusion at extended defects. Prog. Photovolt., Res. Appl. 21 (7), 1444–1453. http://dx.doi.org/10.1002/pip.2220.

Carr, A.J., de Groot, K., Jansen, M.J., Bende, E., van Roosmalen, J., Okel, L., Eerenstein, W., Jonkman, R., van der Sanden, R., Bakker, J., et al., 2015. Tessera: Scalable, shade robust module. In: 2015 IEEE 42nd Photovoltaic Specialist Conference. PVSC, IEEE, pp. 1–5. http://dx.doi.org/10.1109/PVSC.2015.7356286.

Chan, D.S., Phang, J.C., 1987. Analytical methods for the extraction of solar-cell single- and double-diode model parameters from IV characteristics. IEEE Trans. Electron Devices 34 (2), 286–293. http://dx.doi.org/10.1109/T-ED.1987.22920.

Charles, J.-P., Bordure, G., Khoury, A., Mialhe, P., 1985. Consistency of the double exponential model with physical mechanisms of conduction for a solar cell under illumination. J. Phys. D: Appl. Phys. 18 (11), 2261. http://dx.doi.org/10.1088/0022-3727/18/11/015.

Chegaar, M., Hamzaoui, A., Namoda, A., Petit, P., Aillerie, M., Herguth, A., 2013. Effect of illumination intensity on solar cells parameters. Energy Procedia 36, 722–729. http://dx.doi.org/10.1016/j.egypro.2013.07.084.

Chenni, R., Makhlouf, M., Kerbache, T., Bouzid, A., 2007. A detailed modeling method for photovoltaic cells. Energy 32 (9), 1724–1730. http://dx.doi.org/10.1016/j.energy.2006.12.006.

Deline, C., Meydbray, J., Donovan, M., Forrest, J., 2012. Photovoltaic Shading Testbed for Module-Level Power Electronics. Technical Report, (NREL/TP-5200-54876), National Renewable Energy Lab.(NREL), Golden, CO (United States), http://dx.doi.org/10.2172/1045715.

Eerenstein, W., Jansen, M., de Groot, K., Carr, A., Okel, L., Goris, M., van Roosmalen, J., Bende, E., Jonkman, R., van der Sanden, R., et al., 2015. TESSERA: Maximizing PV yield performance with size flexibility for BIPV. In: 30th European PV Solar Energy Conference and Exhibition. p. 2208. http://dx.doi.org/10.4229/EUPVSEC20152015-5BV.2.13.

Faiman, D., 2008. Assessing the outdoor operating temperature of photovoltaic modules. Prog. Photovolt., Res. Appl. 16 (4), 307–315. http://dx.doi.org/10.1002/pip.813.

Hanifi, H., Dassler, D., Schneider, J., Turek, M., Schindler, S., Bagdahn, J., 2016. Optimized tab width in half-cell modules. Energy Procedia 92, 52–59. http://dx.doi.org/10.1016/j.egypro.2016.07.009.

Hanifi, H., Pander, M., Jaeckel, B., Schneider, J., Bakhtiari, A., Maier, W., 2019. A novel electrical approach to protect PV modules under various partial shading situations. Sol. Energy 193, 814–819. http://dx.doi.org/10.1016/j.solener.2019.10.035.

Hanifi, H., Schneider, J., Bagdahn, J., 2015. Reduced shading effect on half-cell modules–measurement and simulation. In: 31th European Photovoltaic Solar Energy Conference and Exhibition, Hamburg. pp. 2529–2533. http://dx.doi.org/10.4229/EUPVSEC20152015-5CV.2.25.

Hasyim, E.S., Wenham, S., Green, M., 1986. Shadow tolerance of modules incorporating integral bypass diode solar cells. Solar Cells 19 (2), 109–122. http://dx.doi.org/10.1016/0379-6787(86)90036-0.

IRENA, 2018. Renewable Power Generation Costs in 2018. Technical Report, International Renewable Energy Agency, Abu Dhabi.

Ishaque, K., Salam, Z., Taheri, H., et al., 2011. Modeling and simulation of photovoltaic (PV) system during partial shading based on a two-diode model. Simul. Model. Pract. Theory 19 (7), 1613–1626. http://dx.doi.org/10.1016/j.simpat.2011.04.005.

Jäger-Waldau, A., 2019. PV Status Report 2019. Technical Report, (JRC118058), Institute for Energy and Transport, Renewable Energy Unit.

Jahn, U., Nasse, W., 2004. Operational performance of grid-connected PV systems on buildings in Germany. Prog. Photovolt., Res. Appl. 12 (6), 441–448. http://dx.doi.org/10.1002/pip.550.

Kammen, D.M., Sunter, D.A., 2016. City-integrated renewable energy for urban sustainability. Science 352 (6288), 922–928. http://dx.doi.org/10.1126/science.aad9302.

King, D., Boyson, W., J.A., K., 2004a. Photovoltaic Array Performance Model. Technical Report, (SAND2004-3535), Sandia National Laboratories.

King, D.L., Kratochvil, J.A., Boyson, W.E., 2004b. Photovoltaic Array Performance Model. Technical Report, (SAND2004-3535), Sandia National Laboratories, http://dx.doi.org/10.2172/919131.

Kost, C., Shammugam, S., Jülch, V., Nguyen, H.-T., Schlegl, T., 2018. Levelized Cost of Electricity Renewable Energy Technologies. Fraunhofer Institute for Solar Energy Systems ISE.

Lefevre, B., Peeters, S., Poortmans, J., Driesen, J., 2017. Predetermined static configurations of a partially shaded photovoltaic module. Prog. Photovolt., Res. Appl. 25 (2), 149–160. http://dx.doi.org/10.1002/pip.2834.

Lu, F., Guo, S., Walsh, T.M., Aberle, A.G., 2013. Improved PV module performance under partial shading conditions. Energy Procedia 33, 248–255. http://dx.doi.org/10.1016/j.egypro.2013.05.065.

MacAlpine, S.M., Erickson, R.W., Brandemuehl, M.J., 2012. Characterization of power optimizer potential to increase energy capture in photovoltaic systems operating under nonuniform conditions. IEEE Trans. Power Electron. 28 (6), 2936–2945. http://dx.doi.org/10.1109/TPEL.2012.2226476.

Mishra, S., Ziar, H., Isabella, O., Zeman, M., 2019. Selection map for PV module installation based on shading tolerability and temperature coefficient. IEEE J. Photovolt. 9 (3), 872–880. http://dx.doi.org/10.1109/JPHOTOV.2019.2900695.

Mittag, M., Pfreundt, A., Shahid, J., Wöhrle, N., Neuhaus, D.H., 2019. Techno-economic analysis of half cell modules: The impact of half cells on module power and costs. In: 36th European Photovoltaic Solar Energy Conference and Exhibition. EU PVSEC, pp. 1032–1039. http://dx.doi.org/10.4229/EUPVSEC20192019-4AV.1.20.

Mohammadnejad, S., Khalafi, A., Ahmadi, S.M., 2016. Mathematical analysis of total-cross-tied photovoltaic array under partial shading condition and its comparison with other configurations. Sol. Energy 133, 501–511. http://dx.doi.org/10.1016/j.solener.2016.03.058.

Pannebakker, B.B., de Waal, A.C., van Sark, W.G., 2017. Photovoltaics in the shade: One bypass diode per solar cell revisited. Prog. Photovolt., Res. Appl. 25 (10), 836–849. http://dx.doi.org/10.1002/pip.2898.

Perez, R., Seals, R., Michalsky, J., 1993. All-weather model for sky luminance distribution—preliminary configuration and validation. Sol. Energy 50 (3), 235–245. http://dx.doi.org/10.1016/0038-092X(93)90017-I.

Remund, J., Müller, S., Schmutz, M., Barsotti, D., Studer, C., Cattin, R., 2020. Handbook Part I: Software. Meteotest.

Santbergen, R., Muthukumar, V., Valckenborg, R., van de Wall, W., Smets, A., Zeman, M., 2017. Calculation of irradiance distribution on PV modules by combining sky and sensitivity maps. Sol. Energy 150, 49–54. http://dx.doi.org/10.1016/j.solener.2017.04.036.

Silvestre, S., Boronat, A., Chouder, A., 2009. Study of bypass diodes configuration on PV modules. Appl. Energy 86 (9), 1632–1640. http://dx.doi.org/10.1016/j.apenergy.2009.01.020.

Sinapis, K., Tzikas, C., Litjens, G., Van den Donker, M., Folkerts, W., Van Sark, W., Smets, A., 2016. A comprehensive study on partial shading response of c-Si modules and yield modeling of string inverter and module level power electronics. Sol. Energy 135, 731–741. http://dx.doi.org/10.1016/j.solener.2016.06.050.

Solar, A.E., 2019. AE Solar hot-spot free monocrystalline PV modules. (AES-DS2019), URL https://ae-solar.com/wp-content/uploads/2018/10/AE-M6-60-305W-320W.pdf. V.002.

Texas Instruments, 2012. SM74611 smart bypass diode. (SNVS903B), URL https://www.ti.com/lit/gpn/sm7461. Rev. B.

Wolf, M., Noel, G., Stirn, R.J., 1977. Investigation of the double exponential in the current—voltage characteristics of silicon solar cells. IEEE Trans. Electron Devices 24 (4), 419–428. http://dx.doi.org/10.1109/T-ED.1977.18750.

Ziar, H., Asaei, B., Farhangi, S., Korevaar, M., Isabella, O., Zeman, M., 2017. Quantification of shading tolerability for photovoltaic modules. IEEE J. Photovolt. 7 (5), 1390–1399. http://dx.doi.org/10.1109/JPHOTOV.2017.2711429.